

PROCEEDINGS OF SPIE

[SPIDigitalLibrary.org/conference-proceedings-of-spie](https://spiedigitallibrary.org/conference-proceedings-of-spie)

Arcus: an ISS-attached high-resolution x-ray grating spectrometer

R. K. Smith, M. Ackermann, R. Allured, M. W. Bautz, J. Bregman, et al.

R. K. Smith, M. Ackermann, R. Allured, M. W. Bautz, J. Bregman, J. Bookbinder, D. Burrows, L. Brenneman, N. Brickhouse, P. Cheimets, A. Carrier, M. Freeman, J. Kaastra, R. McEntaffer, J. Miller, A. Ptak, R. Petre, G. Vacanti, "Arcus: an ISS-attached high-resolution x-ray grating spectrometer," Proc. SPIE 9144, Space Telescopes and Instrumentation 2014: Ultraviolet to Gamma Ray, 91444Y (24 July 2014); doi: 10.1117/12.2062671

SPIE.

Event: SPIE Astronomical Telescopes + Instrumentation, 2014, Montréal, Quebec, Canada

Arcus: an ISS-attached high-resolution X-ray grating spectrometer

R. K. Smith¹, M. Ackermann², R. Allured¹, M. W. Bautz³, J. Bregman⁴, J. Bookbinder¹, D. Burrows⁵, L. Brenneman¹, N. Brickhouse¹, Peter Cheimets¹, A. Carrier⁶, M. Freeman¹, J. Kaastra⁷, R. McEntaffer⁸, J. Miller⁴, A. Ptak⁹, R. Petre⁹, G. Vacanti², and the Arcus team

¹Smithsonian Astrophysical Observatory, ²cosine Research, ³Massachusetts Institute of Technology, ⁴University of Michigan, ⁵Pennsylvania State University, ⁶Lockheed-Martin Advanced Technology Center, ⁷SRON, ⁸University of Iowa, ⁹NASA Goddard Space Flight Center

ABSTRACT

We present the design and scientific motivation for Arcus, an X-ray grating spectrometer mission to be deployed on the International Space Station. This mission will observe structure formation at and beyond the edges of clusters and galaxies, feedback from supermassive black holes, the structure of the interstellar medium and the formation and evolution of stars. The mission requirements will be $R > 2500$ and $> 600 \text{ cm}^2$ of effective area at the crucial O VII and O VIII lines, values similar to the goals of the IXO X-ray Grating Spectrometer. The full bandpass will range from 8-52 Å (0.25-1.5 keV), with an overall minimum resolution of 1300 and effective area $> 150 \text{ cm}^2$. We will use the silicon pore optics developed at cosine Research and proposed for ESA's Athena mission, paired with off-plane gratings being developed at the University of Iowa and combined with MIT/Lincoln Labs CCDs. This mission achieves key science goals of the New Worlds, New Horizons Decadal survey while making effective use of the International Space Station (ISS).

Keywords: gratings, ISS, instrumentation, X-rays: spectroscopy

1. INTRODUCTION

The highly energetic processes involved in the formation of galaxies and clusters, the outflows from supermassive black holes, and stellar corona magnetospheres all leave signatures in the form of highly ionized metals with characteristic temperature, density, and velocity distributions. The X-ray gratings on Chandra (HETG, LETG) and the XMM-Newton (RGS) satellites have sampled, with long observations of the brightest objects, some of the science enabled by high-resolution soft X-ray spectroscopy^{1,2,3,4,5}. The current generation of X-ray gratings, however, have only modest resolutions ($R \sim 200$ -1200) and efficiencies of only a few percent, limiting most studies to only a few sources. To make substantial progress in this area, a major leap in capabilities, both resolution and effective area, will be required. Fortunately, recent advances in grating technology and X-ray optics have enabled such a leap at a modest cost, as shown in Figures 1, 2, and 3. Arcus (Latin for 'arc' or 'rainbow') is a proposed SMEX (\$125M cap) mission to be installed on the ISS. It will use the off-plane gratings⁶ that have been under development for Constellation-X and IXO⁷, combined with the silicon pore optics⁸ planned for use on ESA's upcoming Athena mission. The focal plane will use the current generation of CCDs based on the Suzaku⁹ design, with electronics similar to that of Swift¹⁰ and the upcoming TESS¹¹ mission; the pointing system and mission operations will be similar to those planned for NICER¹². We describe below the science, instrumentation, and operations plan for Arcus.

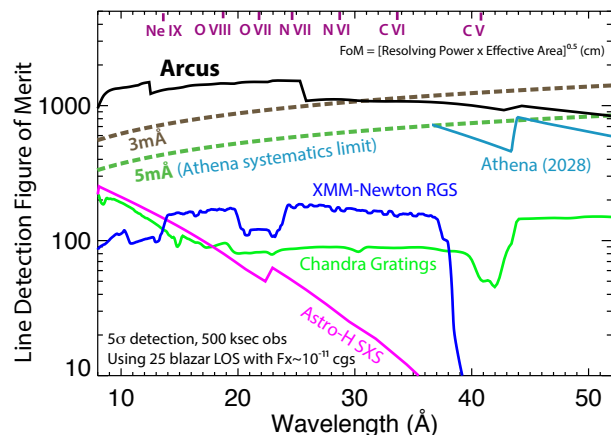


Figure 1 – Arcus figure of merit for detecting weak lines compared to existing and future missions.

2. THE SCIENCE OF ARCUS

The soft X-ray bandpass from 8-52 Å contains strong transitions from abundant atoms and ions over a broad range of temperatures and ionization parameters, enabling studies of a wide variety of science topics. During the prime mission, we will focus on three specific areas: structure formation, supermassive black hole (SMBH) feedback, and stellar formation and evolution. We briefly describe our specific science plans for each area here.

Table 1: Arcus Science Traceability Matrix

Topic	Science Goals	Measurement	Requirement
Structure Formation	Trace metals beyond virial radius to test formation theories.	Survey absorption lines of 50 galaxies and clusters to 3x virial radius. Survey 50 LoS through Galactic Halo & Local Group to find structure, abundance. Measure abundances, velocities, & composition within Milky Way.	600 cm ² at O VII, 150 cm ² minimum effective area throughout, with 8 Msec of observing time. R>1500 over 12-40Å bandpass to get C, N, O, and Ne ions. R>2500 at O VII
SMBH Feedback	Measure mass & energy in outflowing SMBH wind.	Observe absorption and emission lines from range of ions to measure velocities & profiles and temporal variation in response to changing SMBH flux.	Bandpass 8-52Å with >150 cm ² EA throughout, R>1500 and an observing time of 8Msec.
Stellar Life Cycle	Determine how young stars dispersed their disks.	Map T _c and n _e , absorption column of pre-shock gas, and v _{turb} vs shock cooling.	Bandpass 8-52Å with >250 cm ² EA throughout, R>1500 and an observing time of 4Msec.

2.1 Structure Formation

The natural outcome of the formation of structure is the production of hot gas (10⁵–10⁸K) on the scales of galaxies, galaxy groups and clusters, as well as the collapsing intergalactic filaments that comprise the cosmic web (the ‘Warm-Hot Intergalactic Medium’ or WHIM). The importance of this gas is not simply that it accounts for about half of the baryons in the Universe, but its properties encode the processes that lead to structure formation and evolution. The study of the WHIM is sometimes trivialized as the search for the missing baryons. As mass is conserved, the baryons cannot be missing, but it is the distribution of the baryons with temperature that is crucial in revealing the physical processes relevant to the formation of large-scale structure as well as galaxy formation. For example, the formation of galaxies produces a large number of massive stars and supernovae, along with a central SMBH. These heat the accreting gas in different ways, and although galaxy formation models predict hot extended gaseous halos, there is enormous model variation in the predicted gas mass, temperature and abundance distributions. These vital properties are largely unconstrained due to the lack of relevant data. Arcus will provide the critical data that will identify the correct astrophysical models for galaxy and larger scale structure formation.

In cosmological simulations, the collapse of dark matter filaments is collisionless, but the gaseous component undergoes shocks, heating the gas to WHIM temperatures. The intersections of cosmic filaments are nascent galaxy clusters that grow through the continued inflow from the matter in the connective filaments. The galaxy clusters become virialized (overdensity above 200), but they are difficult to study in emission at radii greater than about half the virial radius. At larger radii, the filaments are non-virialized structures, and where they feed the clusters, their overdensities are predicted to be typically 30-200. This formation of structure model for galaxy clusters has yet to be tested, as information on hot gas near and beyond the virial radius has been extremely challenging to obtain. However, the WHIM absorption studies proposed here can trace both the outer parts of clusters as well as the baryonic filaments that drain into the galaxy clusters.

The evolution of cold dark matter is probably simple as it is just the gravitational response to a perturbation spectrum that is measured from the CMB. The complications arise in the baryonic component, which undergoes heating and cooling, and can undergo a variety of fluid phenomena, including shocks and turbulence. In addition to the shock heating associated with accretion, further heating occurs from supernovae of massive stars and from AGNs. The amount of additional entropy provided by stars and AGNs is not easily calculated, so for simulations that study cluster evolution, a “preheating event” is usually assumed to occur at a redshift when the cluster was just about to form¹³ (i.e., z ~ 3). A second and very important consequence of the preheating event is that stars will not only heat the gas, they will pollute their surrounding with metals. These supernova pro-

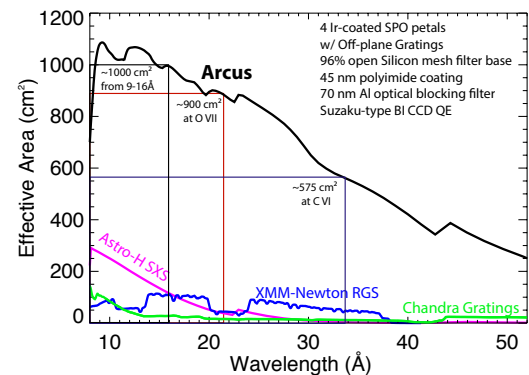


Figure 2 – Arcus effective area compared to existing and future missions.

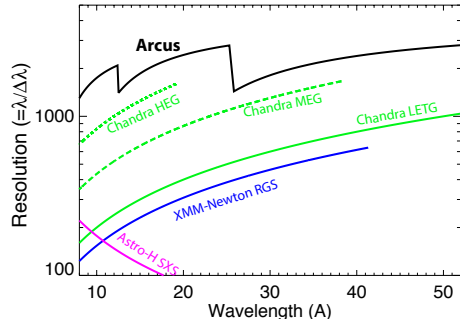


Figure 3 – Arcus Resolution compared to other missions

galaxy groups, we might expect similar or higher metallicities, as there are relatively more stars compared with the gas mass.

A measurable X-ray absorption line in the continuum of a background AGN is produced with a column of about $3 \times 10^{19} \text{ cm}^{-2}$ for a metallicity of 0.2 solar. The ions of interest must lie in the 0.25-1.5 keV range and the strongest lines come from the abundant elements of C, N, O, and Ne, along with Fe L ions such as Fe XVII. The ions with X-ray transitions in this band are tracers of gas in the $3 \times 10^5 - 10^7 \text{ K}$ range, with the upper limit being set by the relevant ion becoming completely ionized. This temperature corresponds to the outer parts of galaxy groups, poor clusters and to the unvirialized material in the cosmic web filaments before the material reaches the virial shock in clusters.

More quantitative predictions require simulations, which have been carried out in cosmological models, for the strongest expected resonance lines of O VII and O VIII (0.574 keV and 0.653 keV). These models predict that with sight lines toward a moderate number of X-ray bright background AGNs, we will detect about 40 absorption line systems. For systems where we measure multiple ions, we can determine the temperature, and by applying the models, infer the metallicity as well as the mass. The application of simulations to the Ly α lines of HI has been highly successful in determining the mass of that cooler component, so we have every expectation that this application to X-ray absorption lines will meet with success.

2.2 Supermassive Black Hole Feedback

Supermassive black holes (SMBHs) play a poorly-understood role in shaping galaxy and cluster formation. Multiple lines of evidence show a strong connection between SMBH mass and galaxy size, so somehow larger galaxies lead to greater SMBH growth. At the same time, winds from SMBH must expel gas from galaxies, cutting off star formation and, in all likelihood, the SMBH growth process. Many questions remain, however, about this feedback process, including

1. How and where are winds launched?
2. What is the acceleration mechanism?
3. What is the structure of these winds?
4. How much mass and energy do they carry away?
5. What is their composition?

Questions 1 & 2 are strongly related. A key goal is here to find the distance of the wind to the SMBH. Is it close to the accretion disk, or to the dusty torus region? The distance can be deduced

genitors are expected to be high mass stars, so the resulting supernovae produce large amounts of heavy elements, notably O, C, N, Fe, S, Si, and Ne. It is these pollutants that produce the WHIM absorption lines, so by measuring them, we not only determine the distribution and mass of the gas, we determine its enrichment properties and thereby the energy input provided by stars in the preheating event.

The few metallicity measurements that we have for the outer parts of galaxy clusters demonstrate that Arcus can measure absorption line features. In a major effort for the Perseus cluster, Werner et al.¹⁴ stitched together many pointings with the Suzaku X-ray telescope to determine the temperature and metallicity with radius. The metallicity, as measured from Fe emission lines, decreases with distance from the center but flattens at large radius to a value of about 0.3 solar. For poorer clusters, such as

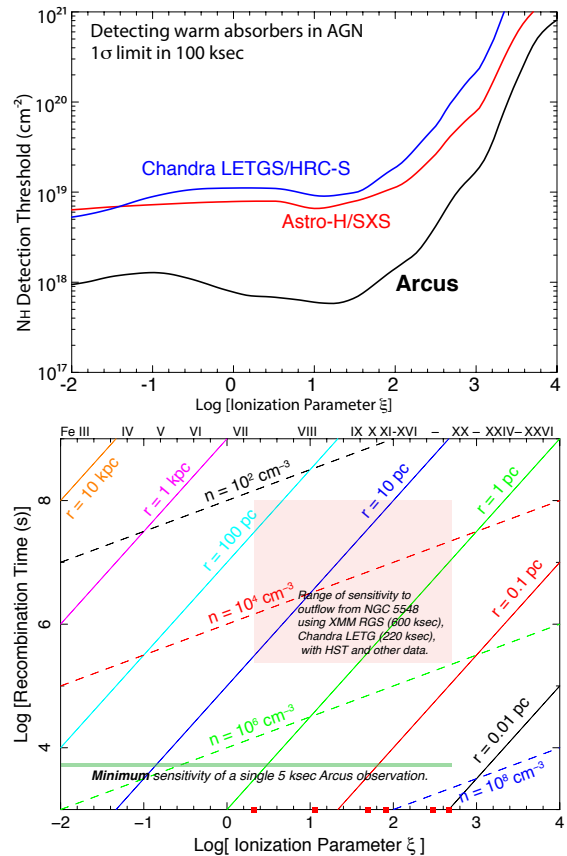


Figure 4 – [Top] Arcus's ability to detect absorbing photoionized plasmas compared to other missions/ [Bottom] Recombination time scale for iron ions vs. ionization parameter in NGC 5548. Arcus will sample timescales from a few hours up to a few years. Solid lines indicate distance from the black hole, dashed lines hydrogen density; the Fe ions at their peak concentration are shown at top.

from the X-ray spectra which give the ionization parameter ξ and a measurement of the density. This density can be obtained by measuring how fast the gas recombines in response to continuum changes. At present this is possible for only a few of the brightest AGN with XMM-Newton using exposure times of >500 ks. Using Arcus, with both 10x better effective area and spectral resolution, this can be achieved in ~5 ks for the brightest sources, or in 500 ks for 100 times dimmer sources (see Figure 4 [Top]).

Regarding the structure of the wind, UV observations like those with HST/COS resolve outflows in velocity space down to a few tens of km/s. In several sources we see multiple UV velocity components, separated by several tens to a few hundred km/s. However, UV observations only measure the gas of lowest ionization. We now know that the bulk of the outflow has higher ionization degree and is only visible in X-rays. Unfortunately, the spectral resolution of the present generation grating spectrometers is of order 1000 km/s, or at best a few hundred km/s. Neither Astro-H nor Athena will improve this situation (except partially near the Fe-K complex). With Arcus's spectral resolution of 100 km/s we can fully characterize the two-dimensional ionization-velocity plane and deduce the structure of the outflow. As shown in Figure 4 [Bottom], monitoring of selected sources during the Arcus mission will determine also the density and location of all components. Using this information about distances, velocities, and densities, both the mass outflow rate as well as the kinetic luminosity of the outflow will be known, and these can be compared to the net accretion rate as derived from the observed continuum properties of these AGN. Finally, accurate chemical composition of the wind can be derived only for the brightest few AGN using Msec exposure times with XMM-Newton or Chandra, and then only for a small number of elements (typically C, N, O, Ne, Mg, Si, S, Fe). With Arcus we can obtain abundances for several other elements in these bright sources, or obtain abundances in a much larger sample of dimmer sources, allowing us to study the conditions for star formation close to the nucleus in detail, and to assess the chemical composition of the outflow that reaches large distances from the active nucleus.

2.3 Stellar Life Cycles

Young stars show high levels of magnetic activity relative to their main sequence counterparts, which may result from a more active stellar dynamo, a conclusion reached from surveys of star forming regions where the coronal emission dominates, or in the case of accreting systems, may be accretion-driven, processes only visible using high resolution soft X-ray spectra. About a dozen young stars have been observed using the Chandra and XMM-Newton gratings. While these observations have confirmed the basic accretion shock model – temperature and density measurements from Ne IX and O VII indicate high densities at relatively low temperatures compared with pure stellar coronae – what happens when the shocked gas approaches the stellar atmosphere is an open question. The standard model suggests a gentle slowing down and cooling of the post-shock plasma, but unexplained phenomena abound, such as events in H and He lines triggered by X-ray events, far too much O VII, and UV line profiles that resist efforts at modeling. A 2010 Decadal panel report noted “High-resolution spectroscopy in the UV from FUSE and HST/STIS and X-ray regimes would significantly sharpen the understanding of how accretion flows arrive on the surface of a star, with implications for the star’s angular momentum, and for its accretion luminosity, which controls the ionization of the planet-forming regime in the disk.” (p. 179)

Arcus can map the temperature and density of the post-shock gas, determine the absorbing column, which is likely to be the accretion streams, and most importantly measure any non-thermal line broadening associated with the turbulent interaction, all highly relevant topics in star and planet formation. Accreting young stars are spinning too slowly, given the fact that they are still contracting and material is being dumped on them – but where does the angular momentum go? Models are still an order of magnitude away from being able to account for this, but accretion-driven magnetic waves at the stellar surface are a serious contender. A young star’s magnetic field and high energy radiation are also important for planet formation – ionizing the disk and driving the magnetorotational instability – and getting enough gas movement in the radial direction for planets to grow. Furthermore, the gas in the disk goes away very

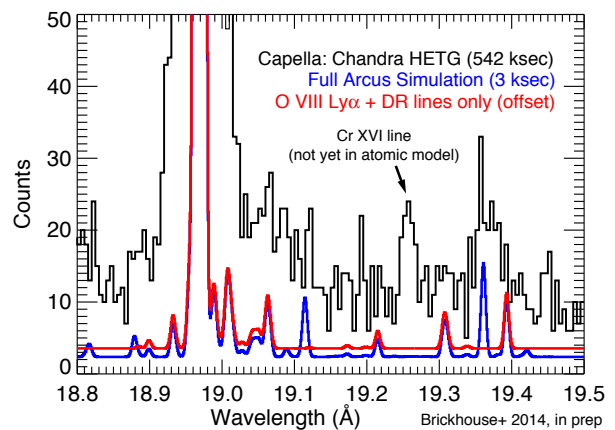


Figure 5 – Capella observed with Chandra’s HETG compared to an observation < 1% as long with Arcus.

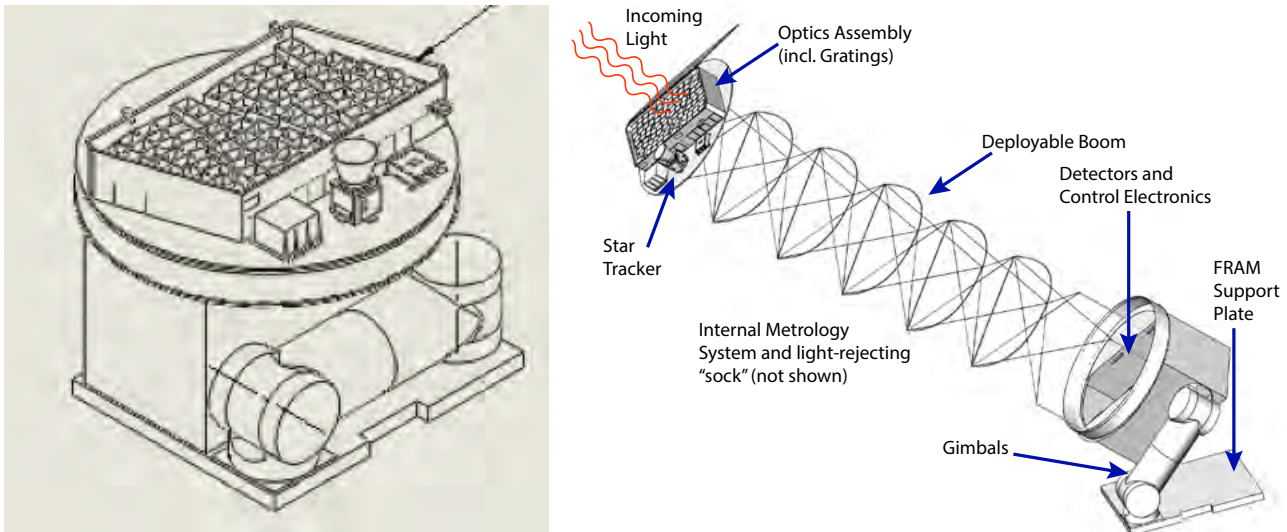


Figure 6 – [Left] Arcus in its stowed configuration, used for launch and during EVAs or other similar ISS events. [Right] Arcus in its deployed configuration with extendable boom and pointing arm. The boom will have a 'sock' to reject stray solar and other light.

quickly (after ~10 Myr), and planets cannot form without gas.

Main sequence coronal sources also provide a range of open questions, including the mechanism that heats the solar corona to >400x the temperature of the photosphere. Solar physicists now have exquisite spatial and timing resolution, but they only have high resolution spectroscopy in the UV, narrow filter bands in the extreme UV and broad bands in the X-rays. Stars offer a large parameter space for studying stellar coronae, and have already shown coronal structures that defy the magnetic loop structure models developed for the solar corona.

One of the popular coronal heating models developed circa 1990 is the so-called impulsive heating or nanoflare model, where loops are randomly heated by energetic particles. Each loop heats up and ionizes quickly, then cools and recombines very slowly. On average the charge state of the gas lags the local temperature, so the plasma should look like a recombining plasma. Very recently, a predictive Alfvén wave heating model has been proposed with uniform input so the whole loop sees the same heating function. Turbulently-broadened lines and a rather steady, equilibrium plasma are predicted. The very weak dielectronic satellite lines are highly sensitive to a recombining plasma, as they become stronger at lower temperature. As can be seen in Figure 5, we see evidence for these features in the accumulated HETG spectrum of Capella, but they are difficult to measure without higher spectral resolution. With Arcus we will be able to use these diagnostics to test heating models.

3. INSTRUMENTATION

The prime objective of the Arcus instrument is to observe cosmic X-ray sources from the ISS. By basing the instrument on the ISS, we will avoid the cost associated with designing and building a spacecraft, allowing us to maximize the instrumental capabilities. In addition, locating Arcus on the ISS ensures a large power supply and a large data allowance. In exchange, the instrument will be subject to the ISS environment, which includes its structural vibration and physical location limitations including various obstructions on the sky. We describe below a vibration suppression system in combination with a laser metrology system that is being studied to address the issue of vibration in the ISS environment. We will also have size limitations that depend on context: launch configuration and instrument swing limitations due to the ISS.

3.1 Overall Mechanical Design

The instrument, like many X-ray telescopes, consists of a set of optics at one end, a set of detectors at the other, and nothing but support structure in between. The optics consist of three or four 'petals' containing silicon pore optics (SPO) modules manufactured by cosine Research⁸. Each petal holds 25 SPO modules. The SPO modules themselves are made of >40 layers of silicon wafers⁸, assembled to produce a grazing-incidence imaging mirror. To achieve the dispersive spectroscopy, a set of grating modules is mounted and aligned behind the SPO modules. The SPO and grating modules in

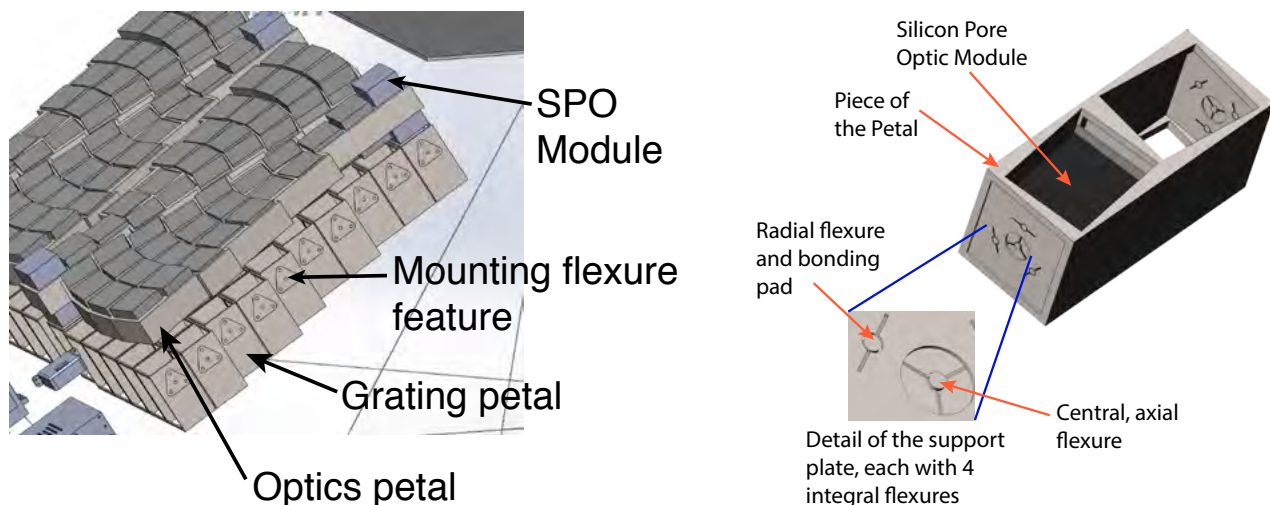


Figure 7 – [Left] Detail of optical module showing four petals interlaced with SPO modules inserted. The gratings, not shown, are mounted directly behind the optics. [Right] Detail of two SPO mounting positions within a petal, highlighting the support plate with multiple integral flexures.

each petal are coaligned to focus a spectrally-dispersed beam on a single detector assembly per petal.

The mechanical design (see Figure 6) is controlled both by the limitations imposed on it by the ISS and by the science requirements it is intended to achieve. In order to accommodate the launch envelope and the on-orbit redeployment requirements, the optics assembly and the detectors are held by an ATK deployable boom. The baseline boom is a coilable system similar to the boom designed for the GEMS SMEX. The boom will be either 3- or 4-sided, and be covered with a fabric sock that prevents stray X-rays from hitting the focal plane and controls thermal radiation. The detector end of the instrument consists of an enclosure that carries the detectors, control electronics, and thermal control and radiator components. The entire instrument is oriented by a two-axis gimbal system, with the possible inclusion of a 6 DOF vibration isolator.

In the launch configuration, the three-petal version instrument fits onto the standard transport and interface plate associated with ISS-deployable instruments, called a Flight Releasable Attachment Mechanism (FRAM). A possible four-petal configuration (shown in Figure 7 [Left]) meets the launch envelope's 1.1m height requirement (from the FRAM base to the top of the instrument) but slightly overhangs the sides of the FRAM. There is also a reusable door that closes off the optics modules for launch and instrument redeployment.

The star tracker pointing control sensors are mounted with the optical modules, and therefore witness any boom bending that occurs as a result of either ISS vibration or pointing-induced torque noise. To measure motions of the detector plane relative to the optics we plan to use a metrology system based on one developed for the Astro-H system¹⁵. By tracking the relative motion of the optics platform with respect to the detectors in the two lateral linear degrees of freedom as well as roll about the optical axis at a frequency higher than the expected modes of the boom, we can reconstruct the photon arrival position on the CCD, as is done on Astro-H.

3.2 Off-Plane Gratings

Off-plane reflection grating spectrometers offer preferable telescope packing geometries compared to the more standard in-plane design, excellent throughput, and high resolving power for soft X-rays. Placed in the converging beam of a focusing X-ray telescope, an array of gratings positioned in the off-plane mount disperses the converging light into a cone and forms an arc of diffracted light at the focal plane⁶. The dispersed spectrum is then imaged by a detector, typically a CCD camera.

Figure 8 illustrates the diffraction geometry that achieves these advances. The optical axis extends out of the page and X-ray photons nominally converging to a telescope focus are instead intersected by an off-plane grating in a direction nearly parallel to the grooves. This creates an arc of diffraction at the focal plane with dispersion dictated by the displayed grating equation. The grating grooves are shown projected from the position of the gratings all the way down to the focal plane. This distance is called the throw and is typically several meters. Obtaining high reflectivities of the X-rays necessitates grazing incidence and, in turn, arrays of aligned, stacked gratings. Such an array can obtain optimal

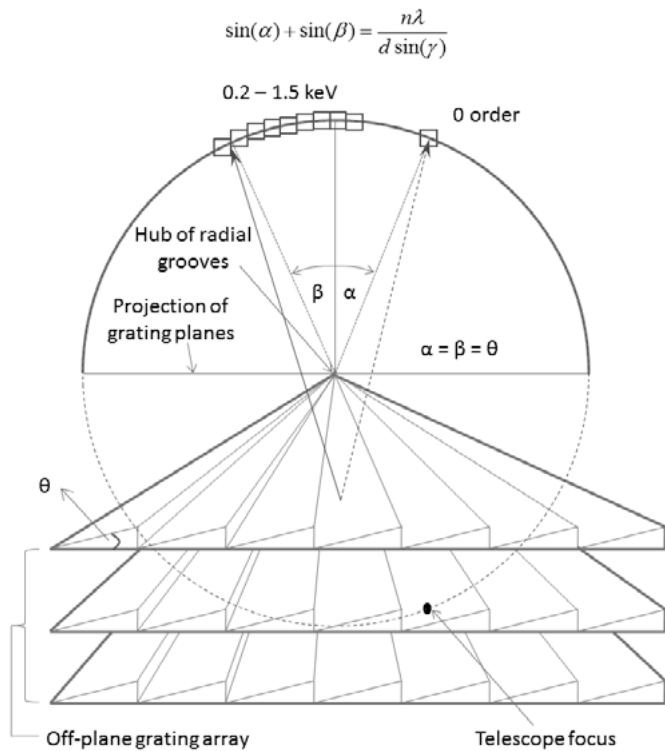


Figure 8– The off-plane grating geometry is displayed with the optical axis projecting out of the page. Three representative gratings demonstrate the blazed radial profile used to meet performance requirements.

the intersection of the cone of diffraction with the focal plane. This circle also contains both the telescope focus and the zero order focus. The graze angle is maintained over the array by fanning the gratings such that all surfaces intersect the same line when projected to the focal plane, but it is important to note that each grating has its own optimal focal plane. If there are many gratings in an array, then a single focal plane is chosen somewhere within the range of individual focal planes. Therefore, the system is inherently astigmatic.

3.3 Optics and Optical Design

The optical design for Arcus takes advantage of the spectral resolving power benefits gained by subaperturing a telescope¹⁶. Sampling a small azimuthal range results in a bowtie that is as broad as the full shell point spread function (PSF) in the radial direction, but many factors narrower in the azimuthal direction (see Figure 9). Aligning the off-plane dispersion direction to the narrow dimension of the PSF will minimize the width of the line spread function (LSF) and maximize spectral resolving power. The obvious trade-off is collecting area as the azimuthal range is heavily restricted. A raytrace study is necessary to optimize the spectral resolving power while maintaining the largest possible telescope. For Arcus, such a study revealed that a 30° telescope azimuth is capable of producing an adequate telescope PSF, ~1". Once determined, the radial range is optimized to maximize collecting area. A reasonable first estimate for this range can be found by scaling the SPO optics from the Athena designs¹⁷. This results in optics radii ranging from ~100 – 600 mm. Raytracing

collecting area in the off-plane mount given that the grazing angle of incoming light onto the grating is equal to the half angle of the arc of diffraction exiting the grating surface. This allows for closely spaced packing geometries that are not available to traditional in-plane reflection grating arrays, such as those in the XMM RGS. Furthermore, the groove surfaces can be blazed to a triangular profile that preferentially disperses light to one side of zero order. This increases the signal-to-noise for these orders and allows a smaller detector array. The blaze angle (θ in Figure 8) is chosen to optimize diffraction efficiency at a preferred wavelength, typically in the middle of the first order bandpass, which translates to optimized efficiencies at higher orders for shorter wavelengths. The grating array is then placed with the grooves at a slight angle relative to the optical axis resulting in an α for zero order at the focal plane that equals the β of the optimized wavelength. When $\alpha = \beta = \theta$, the array is optimized for diffraction efficiency.

The projection of the grooves in Figure 8 illustrates the radial distribution necessary to achieve high spectral resolving power. The convergence of the grooves matches the convergence of the telescope beam, thus maintaining a constant α at the grating and constant β per wavelength at the focal plane, which limits groove profile induced aberration. The grooves converge to a point at the center of the circle defined by

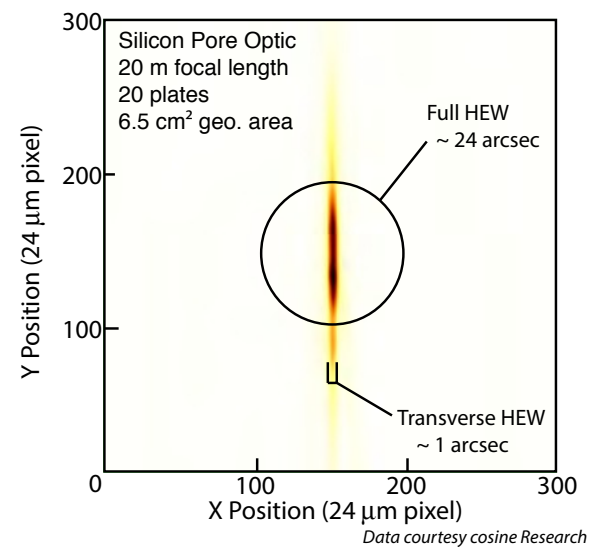


Figure 9 – An SPO optic, showing the characteristic asymmetric PSF. Subaperturing relies upon the small HEW of the transverse PSF rather than the larger full PSF.

the LSF for this range of radii uncovered the major challenge in the optical design of Arcus: its short 5m focal length. This fast beam creates a wide range of angles for the converging light intersecting the grating array, and thus creates a wide range of angles among the optimal grating focal planes. The large astigmatism unacceptably blurs the LSF and limits spectral resolving power. To overcome this limitation we studied and implemented three radial ranges within the grating array over which the 30° subapertured PSF can be maintained. As shown in Figure 8, the three radial ranges are 100–400 mm (R1), 400–550 mm (R2), and 550–660 mm (R3). In each of these ranges the LSF maintains a maximum ~1.7" HPD. If we assume that telescope and alignment errors are randomly distributed in the dispersion direction with a 1" FWHM then we achieve a Gaussian LSF of 2" in each of these radial ranges. Due to the fast speed of this design, each radial range has an independent dispersion focus located at successively deeper foci with higher radii. These planes can be brought to the same position along the optical axis, allowing use of a single CCD detector, using axial offsets such that the telescope optics in R2 are adjusted by 9.39 mm, relative to R1, and those in R3 by 23.64 mm, relative to R1. Therefore, the final design of an optical module consists of a 30° azimuth petal with optics inhabiting radii from 100–660 mm in three radial sections, as seen in Figure 10. The resulting theoretical performance of this design is shown in Figures 1-3. The spectral resolving power varies slightly between R1, R2, and R3 at the 10% level; an average is shown in Figure 3.

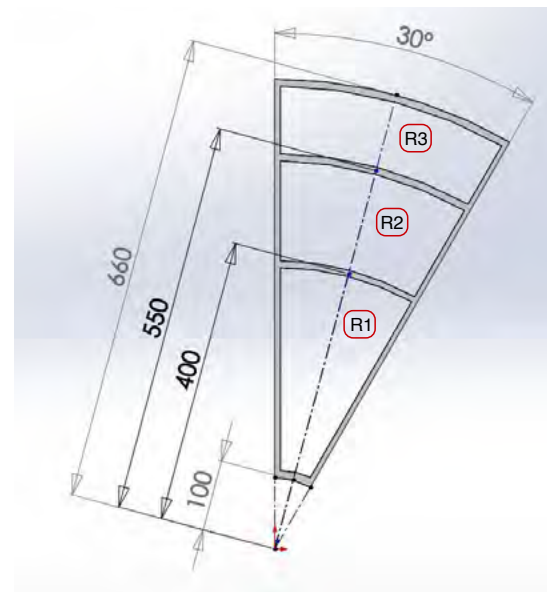


Figure 10 – Arcus optical petal, with lengths in mm.

The Arcus design utilizes radial, blazed gratings with 160 nm groove spacing at a graze angle of 1.5° and a throw of 4.7 m. The blaze angle is 16° to optimize throughput in first order from 25-51Å. The gratings are 100 mm long in the axial direction and 85 mm wide in the dispersion direction. The blaze is obtained by etching down to the <111> crystal plane of a Si wafer^{6,18}. The gratings are aligned within modules which are subsequently aligned and mounted to the petal.

3.4 Mounting the SPO Modules and Grating Modules

The SPO modules are aligned and then bonded into a petal, after which each grating module is mounted and aligned behind an SPO module, as described below. The baseline bonding approach involves a set of flexured bonding pads. There will be three flexured bonding pads on one side of the module and a single flexured bonding pad on the other side of the module. The three flexures on one side are arranged in a triangular pattern, isolating the modules from differential CTE issues between it and the petal (see Figure 7 [Right]). The single flexure on the far side of the module is flexured in the direction toward the three flexure pattern on the far side of the module, isolating the module from the effects of differential CTE in that direction.

To align the SPO modules into a petal structure, a ~ 150 mm diameter collimated beam is used to simultaneously illuminate multiple modules. The diffraction pattern that results from illuminating an entire SPO module with an optical laser produces a narrow focal spot with low-intensity diffraction orders separated by several mm (see Figure 11), allowing for accurate co-alignment. Simultaneous illumination then allows the co-alignment of multiple SPO modules. The collimated beam is translated to illuminate modules as they are added to the petal. A removable reference flat between the petal and the laser source is used to maintain alignment of the collimated beam as it is translated during the process. Once the SPO modules are aligned and bonded, the grating modules are aligned into the system in a similar fashion, this time co-aligning the

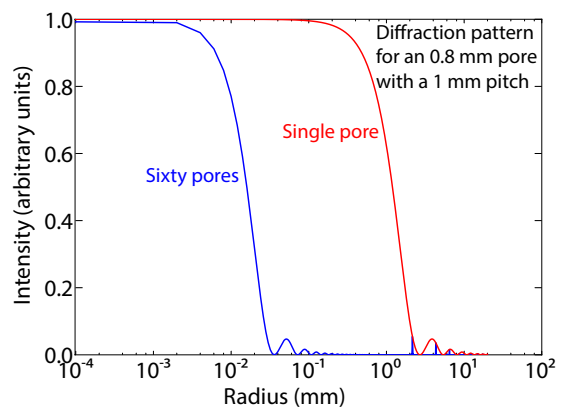


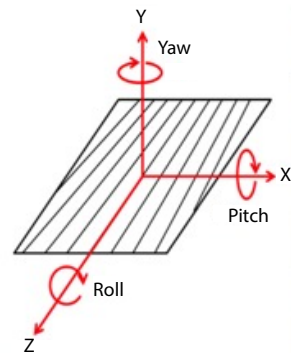
Figure 11: A classical multi-slit diffraction pattern assuming 60 slits (pores) and 440 nm light. This slit pattern is representative of the SPO pore structure, so this estimates the size of the central spot and location of diffracted orders for a fully illuminated SPO module.

zero-order reflections. The yaw angle of the gratings cannot be constrained by reflection of visible light and will instead be monitored by fiducials on each grating module.

The alignment sensitivities for the SPO and grating modules have been calculated and are shown in Table 2. The tightest tolerances are 20 arcsecond rotations and 40 micron translations of the SPO modules. These tolerances were derived following a previously-developed method¹⁹ and verified with the Zemax software package. Our proposed alignment technique is easily capable of reaching these tolerances.

Table 2: Alignment sensitivities, SPO & gratings

Linear DoF	Sensitivity	Rotational DoF	Sensitivity	
Grating	X	±1 mm	Pitch	±30 arcsec
	Y	±1 mm	Yaw	±3 arcmin
	Z	±0.7 mm	Roll	±20 arcsec
SPO	X	±40 μm	Pitch	±0.25 deg
	Y	±1.5 mm	Yaw	±0.25 deg
	Z	±2.5 mm	Roll	±25 arcsec



3.5 Focal Plane and Electronics

The basic architecture of the Arcus Focal Plane Instrumentation is illustrated in Figure 12. Baseline characteristics are listed in Table 3. The major elements are four focal plane modules, two detector electronics assemblies, and a single instrument control unit. We describe each of these in turn.

Focal Plane Modules: Each of the four identical focal plane modules is dedicated to one of the four Arcus spectrometers. Each focal plane module comprises a CCD focal plane, associated Peltier coolers, optical and contamination blocking filters and a door assembly. The focal plane contains a single CCD to record the zeroth order image and two other CCDs to record the dispersed spectrum. Baseline CCD characteristics are listed in Table 3. The spectral readout CCDs are back-illuminated MIT Lincoln Laboratory CCID78 devices shown in Figure 13. These detectors trace heritage directly to those now in operation on both the Chandra X-ray Observatory and on Suzaku. A relatively thin (70nm aluminum) optical blocking layer is deposited directly on the detectors. A single focal plane structure holds all three CCDs within required alignment tolerances. The focal plane is cooled thermo-electrically; the current baseline operating temperature is -90C. Heat is conducted from the warm side of the thermoelectric coolers through the module base and thence to radiators via heatpipes. Each focal plane module is fitted with a filter and door assembly. The thin (45 nm) polyimide filter, supported by a silicon strongback, is maintained at room temperature to protect the focal plane from external contamination. This filter exploits technology developed for sounding rocket instruments by the the University of Wisconsin, which will also be used in the Astro-H mission²⁰. The door is designed to be opened once upon deployment.

Detector Electronics: Each of two detector electronics assemblies serves two focal plane modules. A digital/clock-driver board, an analog signal processing board and a thermoelectric controller board are provided for each FPM. Following design practice for Explorer missions currently in development at MIT (e.g. NICER¹² and TESS¹¹), the digital board includes a micro-coded sequencer implemented in an FPGA as well as discrete current amplifiers for high-capacitance CCD clocks. The digital board also implements a CameraLink serial digital interface to the instrument control unit. The analog board provides a low-voltage implementation of the video signal processing chain operating for Chandra/ACIS and Suzaku/XIS for each CCD output. Operating at 600 kpix s⁻¹, noise referred to CCD input better than 5 electrons, RMS is anticipated. Two nine-pin power cables and two 25-pin LVDS cables are the interface from each detector electronics assembly to the instrument control unit.

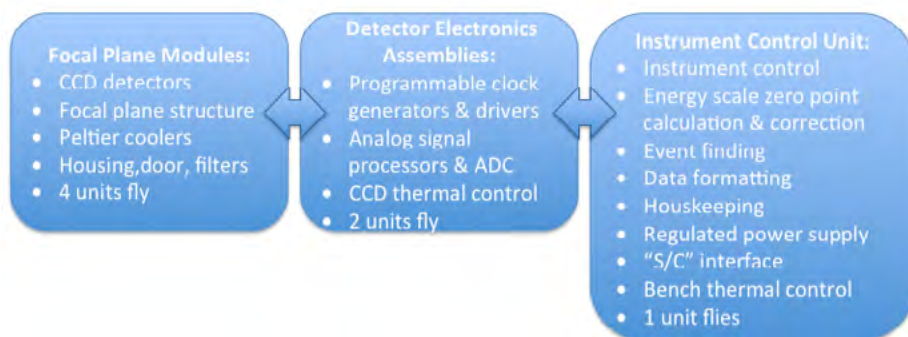


Figure 12: Arcus Focal Plane Instrument Architecture

Table 3: Arcus focal plane instrumentation characteristics

Characteristic/Parameter	Requirement/Value	Remarks
CCD Detectors: Format Pixel size Architecture Outputs/detector	2048 (H) x 1024 (V) pixels 24 μm Framestore, back-illuminated 16	Chandra/Suzaku heritage Samples line response
Focal Plane (each of 4): Spectrum readout area 0th order field of view	24.6 x 99 mm (2 CCDs) 17 x 17 arcmin	Envelopes diffracted spectrum
Readout characteristics: Pixel rate Frame rate Read noise	600 kpix s^{-1} per ch. x 16 channels 10 frames s^{-1} < 5 e^{-1} RMS	16 rows summed on-chip
Filters: Optical block Contamination block	70nm Al 45nm polyimide	Silicon strongback
Digital processing: CPU/rate Event processor	SPARC LEON3FT/100 MHz Xilinx FPGA	

Instrument Control Unit: The Arcus Instrument Control Unit (ICU) is responsible for supplying regulated and unregulated switched power to the instrument (with the exception of the pointing and stowing systems), processing instrument commands, recording instrument housekeeping, extracting X-ray events from the CCD camera datastream, and formatting telemetry. It interfaces to the ISS via power and MIL-STD-1553 buses. The current design features a SPARC LEON3FT processor operating at up to 100 MHz (commandable) with 20 MIPS and 5 MFLOPS.

Event recognition processing is done in a high-speed Xilinx FPGA. CCD bias frames will be stored on-board for each CCD in the instrument. The Event Recognition Processing (ERP) board will perform bias subtraction on the incoming CCD datastream and will then compare each 3x3 group of pixel values to commandable thresholds, grading the pixels according to lookup tables to distinguish between X-ray events and background (charged particle) events. The total non-X-ray background events can be estimated using the experience of the MAXI SSC CCD detector²¹. Valid X-ray events will be formatted for telemetry and send to the ground.

3.6 Pointing Control System

The Arcus pointing system has a deployment function and an inertial optical line-of-sight pointing function. The implementation includes at a minimum a deployment mechanism, a two-axis gimbal, and a star tracker augmented by internal metrology; a 6 DoF vibration isolation system is under consideration. Figure 6 shows diagrams of the instrument and its pointing system in the stowed and deployed configurations. Gimbal deployment is required to move the instrument away from the FRAM so as to provide swing space and a view to celestial targets unobstructed by the surrounding structure. The deployment mechanism is also used to stow the instrument back on the FRAM about once a month during space station events such as re-supply. Pointing control is used to slew the optical line-of-sight of the instrument and track celestial targets. The tracking function compensates for the space station orbital motion and to stabilize the instrument inertial line-of-sight in the presence of space station vibrations and self-induced disturbances. The driving design requirement for the pointing system is the inertial line-of-sight jitter, which is defined as the stability of the instrument optical line-of-sight over any 0.5-second time window. That stability requirement is set at 1-arcsec consistently with the angle subtended by each pixel from the detector.

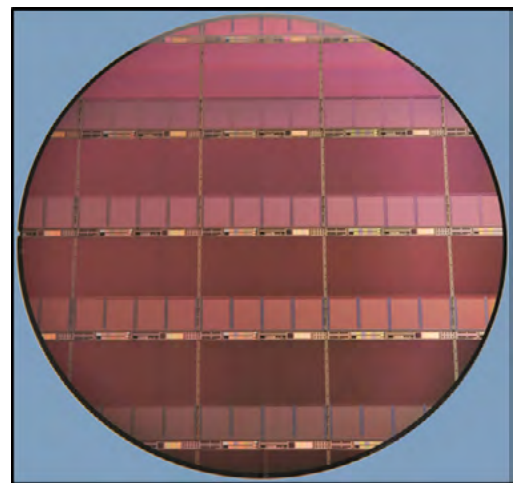


Figure 13 – Baseline Arcus CCDs (MIT/Lincoln CCID78) on 200mm wafer

From a jitter perspective, one major objective of the pointing solution is to mitigate the deflections of the instrument boom (first bending mode estimated at about 4 Hz) under dynamic excitations. Those deflections result in relative motion between the instrument detector and optics modules, which in turn translate into optical line-of-sight jitter. Dynamic excitations include space station vibrations and ripple torques from the pointing system actuators. Another significant source of jitter is star tracker noise, which translates into actuation noise through feedback within the bandwidth of the pointing control system.

We are evaluating two implementation options for line-of-sight pointing. The first option combines a star tracker for inertial line-of-sight sensing and a high-resolution two-axis gimbal for instrument inertial orientation control. The second option combines a star tracker, a coarse-resolution two-axis gimbal, and an active vibration isolation stage between the gimbal and the instrument. The trade is based on launch configuration envelope constraints, mass constraints, and achievable jitter performance.

Option 1: Pointing the payload using two high resolution motors and a star tracker sensor is the most simple, straightforward approach to meeting the Arcus pointing needs. It is the preferred approach, assuming that two conditions can be met: that the ISS base vibrations do not induce unacceptably large boom deflections, and that a set of motors can be identified that have the appropriate performance characteristics, TRL, cost, and size. Initial indications are, that given the measured ISS acceleration levels, the predicted induced LOS errors in the Arcus instrument are near overall allowable values. Motors that achieve the necessary operational precision are large, possibly too large to accommodate the instrument launch envelope. Therefore the inclusion of a 6 DoF isolator is an important design trade.

Option 2: The vibration isolation solution under the second option is based on Lockheed-Martin patented Disturbance Free Payload (DFP) architecture^{22,23,24,25}. In that architecture (Figure 14), aside from electrical power and data cables bridging the interface, the instrument and the gimbal are mechanically isolated, thereby providing a high-degree of vibration attenuation. Beyond some limited range of travel, typically ± 5 -mm in any direction, the instrument is mechanically caged relative to the gimbal so that the two can never fly apart from each other. Using the star tracker output, the instrument inertial orientation is controlled within that limited travel range by commanding a set of 6 large-gap non-contact voice-coil actuators. The gimbal, in turn, is commanded to keep the DFP actuators at or near their center of travel. This architecture permits us to use a set of lower-cost, low-resolution stepper motors for the gimbal, since the DFP isolates the instrument from motor-induced vibrations, while maintaining the needed pointing precision. DFP as a system is at TRL 5 while its components are at TRL 6 or higher. DFP has been demonstrated in multiple laboratory experiments^{24,25} including vibration isolation (up to 68-dB in 1-Hz to 100-Hz), and payload slew and pointing.

Under the DFP option, the jitter performance is limited by the noise of the star tracker used for inertial pointing and residual vibration transmissibility due to the stiffness of the cables bridging the interface between the instrument and the gimbal. Figure 15 shows our preliminary jitter error budget. The Arcus team will choose the baseline pointing control architecture in the next few months based on the predicted cost, TRL, size, weight and performance.

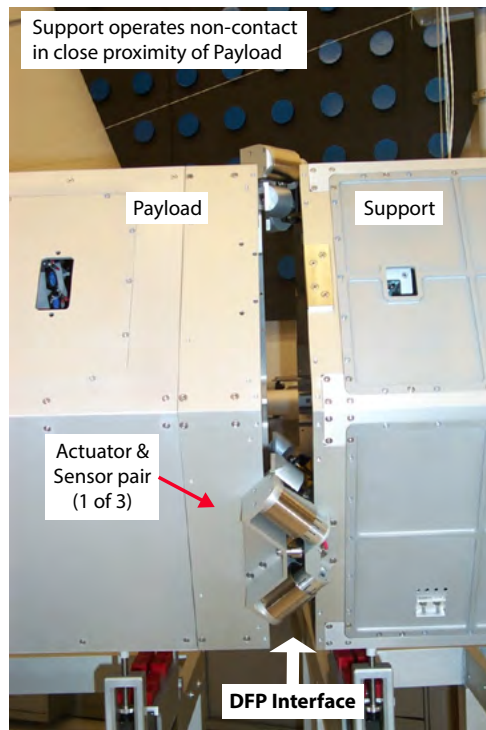


Figure 14 – View of Disturbance Free Payload interface between Payload and Support Module

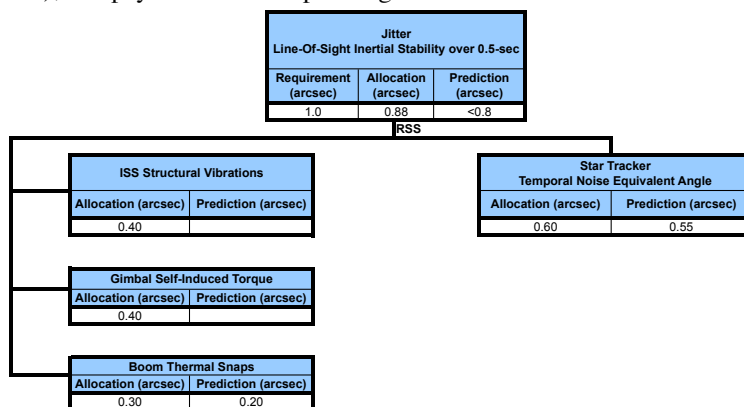


Figure 15: Preliminary jitter error budget

4. CONCLUSIONS

Taking advantage of recent developments in grating technology along with the facilities of the ISS, Arcus can achieve all of the X-ray grating science highlighted by the 2010 Astrophysics Decadal survey within the cost envelope of a SMEX. The Arcus team is highly experienced, having led key aspects of the instrumentation, operations, and science return from the Suzaku, Swift, Chandra and XMM-Newton missions, as well as near-term missions such as NICER and Astro-H.

5. REFERENCES

- [1] Paerels, F. & Kahn, S., “High-Resolution X-Ray Spectroscopy with CHANDRA and XMM-NEWTON”, *ARA&A*, 41, 291-342 (2003)
- [2] Bregman, J. & Lloyd-Davies, E., “X-Ray Absorption from the Milky Way Halo and the Local Group”, *ApJ*, 669, 990-1002 (2007)
- [3] Detmers, R. et al., “Multiwavelength campaign on Mrk 509. III. The 600 ks RGS spectrum: unravelling the inner region of an AGN”, *A&A*, 534, A38 (2011)
- [4] Fang, T. et al., “Confirmation of X-ray Absorption by Warm-Hot Intergalactic Medium in the Sculptor Wall”, *ApJ*, 714, 1715-1724 (2010)
- [5] Brickhouse, N. et al., “X-Ray Determination of the Variable Rate of Mass Accretion onto TW Hydrae”, *ApJL*, 760, 21-26 (2012)
- [6] McEntaffer, R. et al., “First results from a next-generation off-plane X-ray diffraction grating”, *Experimental Astronomy*, 36, 389-405 (2013)
- [7] Bookbinder, J., “An overview of the IXO Observatory”, *SPIE*, 7732, 39 (2010)
- [8] Collon, M et al., “Aberration-free silicon pore x-ray optics”, *SPIE*, 8861, 0 (2013)
- [9] Mitsuda, K., et al., “The X-Ray Observatory Suzaku”, *PASJ*, 59, 1 (2007)
- [10] Gehrels, N. et al., “The Swift Gamma-Ray Burst Mission”, *ApJ*, 611, 1005-1020 (2004)
- [11] Ricker, G. et al., “The Transiting Exoplanet Survey Satellite Mission”, *ArXiv*, 1406.0151 (2014)
- [12] Gendreau, K., Arzoumanian, Z, and Okajima, T., “The Neutron star Interior Composition ExploreR (NICER): an Explorer mission of opportunity for soft x-ray timing spectroscopy”, *SPIE*, 8443, 13 (2012)
- [13] Bialek, J., Evrard, A. E. & Mohr, J. J. “Effects of Preheating on X-Ray Scaling Relations in Galaxy Clusters”, *ApJ*, 555, 597 (2001)
- [14] Werner, N. et al., “A uniform metal distribution in the intergalactic medium of the Perseus cluster of galaxies”, *Nature*, 502, 656-658 (2013)
- [15] Gallo, L. et al., “The Canadian Astro-H metrology system”, *SPIE*, 8443, 54 (2012)
- [16] Cash, W., “X-ray optics - A technique for high resolution imaging”, *Applied Optics*, 26, 2915-2920 (1987)
- [17] Willingale, R. et al., “The Hot and Energetic Universe: The Optical Design of the Athena+ Mirror”, *arXiv*, 1307.1709 (2013)
- [18] Chang, C.-H., Heilmann, R.K., Fleming, R.C., Carter, J., Murphy, E., Schattenburg, M.L., Bailey, T.C., Ekerdt, J.G., Frankel, R.D., Voisin, R.: Fabrication of sawtooth diffraction gratings using nanoimprint lithography. *J. Vac. Sci. Technol. B* 21(6), 2755–2759 (2003)
- [19] Allured, R. & McEntaffer, R. L., “Analytical Alignment Tolerances for Off-Plane Reflection Grating Spectroscopy,” *Experimental Astronomy*, 36, 661, 17 pages, 2013.
- [20] Takahashi, T. et al., “The ASTRO-H X-ray Observatory”, *SPIE*, 8443, 1 (2012)
- [21] Tsunemi, H. et al., “In-Orbit Performance of the MAXI/SSC onboard the ISS,” *PASJ*, 62, 1371 (2010)
- [22] Pedreiro, N., Lockheed Martin Corporation, Bethesda, MD, U.S. Patent for a “Spacecraft Architecture for Disturbance-Free Payload”, US-6454215-B1, filed 29 Jan. 2001, awarded 24 Sep. 2002.
- [23] Pedreiro, N., “Spacecraft Architecture for Disturbance-Free Payload”, *Journal of Guidance Control and Dynamics*, Vol. 26, No. 5, pp. 794-804 (2003)
- [24] Pedreiro, N., Carrier, A.C., Lorell, K.R., Roth, D.E., Shelef, G., Clappier, R., and Gonzales, M.A., “Disturbance-Free Payload Concept Demonstration”, *AIAA Paper 02-5027*, Aug. 2002.
- [25] Gonzales, M.A., Pedreiro, N., Roth, D.E., Brookes, K., and Foster, B.W., “Unprecedented Vibration Isolation Demonstration Using the Disturbance-Free Payload Concept”, *AIAA Paper 04-5247*, Aug. 2004.